

# Nano- versus Micro-sized TiO<sub>2</sub>: Comparative Photoelectrochemical and Photocatalytic Studies towards Organic Pollutants Oxidation in Gas Phase

P. Bonete<sup>a\*</sup>, R. Djellabi,<sup>b</sup> D. Monllor-Satoca,<sup>b</sup> G. Cerrato,<sup>c</sup> L. Operti,<sup>c</sup> R. Gómez,<sup>a</sup> C. L. Bianchi,<sup>b\*</sup>

<sup>a</sup> *Universitat d'Alacant, Institut Universitari d'Electroquímica i Departament de Química Física, Apartat 99, E-03080 Alacant (Spain)*

<sup>b</sup> *Università degli Studi di Milano, Dipartimento di Chimica, via Golgi 19, 20133, Milano, Italy & Consorzio INSTM, via Giusti 9, 50121 Firenze (Italy)*

<sup>c</sup> *Università degli Studi di Torino, Dipartimento di Chimica & NIS Centre of Excellence, via Giuria 7, 10125 Torino (Italy) & Consorzio INSTM, via Giusti 9, 50121 Firenze (Italy)*

\*Corresponding author. Tel: +39 0250314253

Email: [claudia.bianchi@unimi.it](mailto:claudia.bianchi@unimi.it)

\*Co-corresponding author: [pedro.bonete@ua.es](mailto:pedro.bonete@ua.es)

## ABSTRACT

The size of TiO<sub>2</sub> (either nanometric or micrometric) can significantly affect both its photocatalytic and photoelectrochemical properties, thus altering the photooxidation of organic pollutants in air or water. The purpose of this work is to give an account of the photoelectrochemical and photocatalytic features of some nano- and micro-sized TiO<sub>2</sub> commercial powders towards a model reaction, the photooxidation of acetone. Cyclic voltammograms (CV) of TiO<sub>2</sub> particulated electrodes under UV illumination experiments were carried out in either saturated O<sub>2</sub> or N<sub>2</sub> solutions for a direct correlation with the photocatalytic process. In addition, the effect of different reaction conditions on the photocatalytic efficiency under UV light in both aqueous and gaseous phases was also investigated. CV curves with the addition of acetone under UV light showed a negative shift of the photocurrent onset, confirming the efficient transfer of photoproduced reactive oxygen species (ROSs), e.g., hydroxyl radicals, or holes to acetone molecules. The photocatalytic experiments showed that the two nano-sized samples exhibit the best photocatalytic performance. The different photoactivity of the micro-sized samples is probably attributed to their morphological differences, affecting both the amount and distribution of free ROSs involved in the photooxidation reaction.

**KEYWORDS:** nano- and micro-sized TiO<sub>2</sub>; photocatalytic efficiency; photoelectrochemical characterization; environmental remediation

## 1. INTRODUCTION

Semiconductor photocatalysts have been intensively investigated because of their applicability in the treatment of pollutants in both air and water phases. Titanium dioxide ( $\text{TiO}_2$ ), a wide band gap semiconductor (3.0 – 3.2 eV), exhibits an excellent reactivity that enables it to photoabate organic pollutants, ubiquitous in the environment from both natural and anthropogenic origin [1-3]. Moreover, the last decade has witnessed a rapid growth on the nanotechnology field, leading to the increasing use of  $\text{TiO}_2$  nanopowders in industrial and commercial products [4, 5]. The extremely small size of nanopowders crystallites confer them a high specific surface area, which may result in a prospectively greater reactivity compared to larger sized powders [6].

Up to now a widespread attention has been directed to the development of  $\text{TiO}_2$  powders with very small crystallite size in an effort to enhance the photocatalytic activity and process efficiency. However, great concerns have risen in the last years on the effective toxicity of nanoparticles. Particles with diameters below 100 nm fall into the classification of “ultrafine” materials (nanoparticles) [7], and some studies reported these particles are linked with several adverse health effects [8, 9]. Ultrafine particles may be highly harmful for humans because of their capability to deeply penetrate lungs and cell membranes [10] causing lungs tumors, inflammations, fibrosis, DNA damage [11] and cytotoxicity [12, 13]. In order to substitute nano-sized particles in industrial and environmental remediation processes, the current research is investigating the photocatalytic efficiency of  $\text{TiO}_2$  materials possessing larger crystallites size. In particular, some reports have successfully demonstrated the interesting catalytic performance of commercial micro-sized  $\text{TiO}_2$  powders sold as pigmentary materials [14, 15]. The efficiency has been tested towards the photodegradation of (i) both  $\text{NO}_x$  and volatile organic compounds (VOCs) in gas phase, and (ii) some organic dyes dissolved in water [16, 17].

Parallel to this, nanostructured  $\text{TiO}_2$  electrodes have also been extensively studied as photoanodes for photoelectrochemical water splitting [18-21] and water remediation [22-26]. One

peculiar feature of the electrochemical measurements is that the oxidation and reduction reactions can be carried out separately and studied independently. In this way, it becomes possible to gain information on the limiting reaction rate of the individual processes, leading to a clear account of the changes and modifications that could occur on the TiO<sub>2</sub> surface. In several reports, the photoelectrochemical properties of TiO<sub>2</sub> nanoelectrodes were investigated with the aim to study their electronic structure and photoefficiency through electrochemical measurements [27-29]. In particular, the research on the electrochemical properties of TiO<sub>2</sub> electrodes pointed out that the photoefficiency depends on the particle morphology, including size and shape [30-33]. In fact, nanoparticle shape and preferential surface orientation of its facets play an important role in the electrochemical oxidation because these factors affect not only the reactants, but also the interfacial charge transfer. In comparison with their micro-sized counterparts, it is likely that the nano-sized powders suffer from an increased charge recombination rate at the surface, due to the large density of surface states that could act as carrier trapping sites; on the contrary, the micro-sized powders could sustain a built in electric potential within the particle that is able to generate a space charge region that facilitates charge separation, thus preventing surface recombination. Consequently, hindering the recombination of photogenerated charge carriers is essential for improving the efficiency of net charge transfer at the semiconductor/electrolyte interface (SEI). In this respect, many factors can influence the overall electrochemical response, including electrode thickness, surface area and particle size. The correct control of these parameters is thus essential.

The purpose of this paper is to compare the properties of four nano- and micro-sized TiO<sub>2</sub> commercial powders through photoelectrochemical and photocatalytic measurements of the degradation of acetone. In particular, we chose to investigate the oxidation of acetone on TiO<sub>2</sub> as a model reaction to probe its photocatalytic activity. In order to get a correct comparison between electrochemical and photoelectrochemical experiments, the electrochemical analysis was conducted in both saturated N<sub>2</sub> and O<sub>2</sub> solutions; this way, it is possible to independently monitor the reduction

and oxidation processes. In addition, to gain further mechanistic information photoelectrochemical analyses were also conducted for different acetone solution concentrations, investigating the influence of the amount of pollutant on the photoefficiency. The obtained results were finally correlated with the photocatalytic acetone degradation data in order to get a valuable understanding on the photoresponse of the different kinds of commercial TiO<sub>2</sub> powders (nano- and micro-sized) under the chosen photocatalytic conditions. From a wider perspective, the methodology employed in this work could be also extended to the degradation of other substrates.

## **2. EXPERIMENTAL SECTION**

### **2.1. Reagents and chemicals**

Acetone is a Fluka product at high purity grade. Four commercial titanium dioxide samples, two nanometric (AEROXIDE<sup>®</sup> TiO<sub>2</sub> P25 by Evonik Ind. and PC105 by CrystalGlobal) and two micrometric (1077 by Kronos and AH-R by Huntsman), were chosen as photocatalysts and used without any pre-treatment or activation.

### **2.2. Materials characterization**

The surface area of all samples was determined by conventional N<sub>2</sub> adsorption (BET) at 77 K using a Sorptometer instrument (Costech Mod. 1042). X-ray photoelectron spectra (XPS) were taken in an M-probe apparatus (Surface Science Instruments). The source was monochromatic Al K $\alpha$  radiation (1486.6eV). The accuracy of the reported BE can be estimated to be  $\pm 0.2$ eV. The morphology of the catalysts was investigated by high resolution electron transmission microscopy (HR-TEM). TEM images were recorded using a JEOL 3010-UHR instrument (acceleration potential: 300 kV; LaB<sub>6</sub> filament), with samples “dry” dispersed on lacey carbon Cu grids. Absorption/transmission IR spectra have been obtained on a Perkin-Elmer FT-IR System 2000 spectrophotometer equipped with a Hg-Cd-Te cryo-detector in the 7200-580 cm<sup>-1</sup> range at a 2 cm<sup>-1</sup> resolution (number of scans  $\sim 20$ ). For IR

analysis, powder catalyst has been compressed in self-supporting discs (of about  $10 \text{ mg}\cdot\text{cm}^{-2}$ ) and placed in a homemade quartz cell, equipped with KBr windows and connected to a conventional high-vacuum line. Spectra were recorded at room temperature (RT) both in air and after prolonged outgassing at RT.

### 2.3. Preparation of electrodes

TiO<sub>2</sub> electrodes were prepared by spreading an aqueous slurry of commercial nano- or micro-sized TiO<sub>2</sub> over a freshly cleaned conductive glass (fluorine-doped tin oxide, FTO glass). In order to have the same thickness of active material on the FTO surface, the suspension was prepared by adding 0.25 or 0.5 g of TiO<sub>2</sub> powder, respectively for nanoparticles and microparticles of TiO<sub>2</sub>, to a mixture of distilled H<sub>2</sub>O (1.25 mL for nanopowders and 1 mL for micropowders), 15  $\mu\text{L}$  of acetylacetone (Aldrich), and 15  $\mu\text{L}$  of Triton X100 (Aldrich). In general, 15  $\mu\text{L}$  of this suspension were dropped to an FTO glass and a thin film of TiO<sub>2</sub> was obtained using the doctor blade method. Afterwards, the films were annealed and sintered for 2 h at 450°C in air. The average thickness (in  $\mu\text{m}$ ) was measured by means of a Profilometer Instrument (KLA-Tencor Alpha Step D-100) in two different portions of the TiO<sub>2</sub> annealed film.

### 2.4. Photoelectrochemical measurements

The measurements were carried out using a computer-controlled potentiostat (Autolab PGSTAT 30), and a 1000 W Hg-Xe arc lamp (Newport) as an illumination source. The experiments were performed in acidic medium, by using a 0.1 M HClO<sub>4</sub> aqueous solution in a conventional three-electrode photoelectrochemical cell equipped with a quartz window. The counter and reference electrodes were a Pt wire and an Ag/AgCl/KCl (3M) electrode, respectively. All the potentials are quoted against this reference electrode. Before each measurement, the cell was cleaned with an acidic and concentrated KMnO<sub>4</sub> solution overnight, cleaned with a H<sub>2</sub>O<sub>2</sub>/H<sub>2</sub>SO<sub>4</sub> (1:1 vol.) solution and then thoroughly rinsed with distilled water. Finally, the voltammetric cell was boiled in distilled water with a few drops of H<sub>2</sub>SO<sub>4</sub>. The working solution was bubbled with N<sub>2</sub> for 20 min prior to the electrochemical

measurements and then a nitrogen flux was passed over the solution to avoid the oxygen entry. All cyclic voltammograms (CVs) were recorded between  $-0.7$  and  $0.8$  V vs. Ag/AgCl at a scan rate of  $20 \text{ mV}\cdot\text{s}^{-1}$ . For studying the reduction process, the electrolyte solution was saturated with  $\text{O}_2$  by bubbling the gas for 30 min. When the oxidation process was studied, CV measurements of the  $\text{TiO}_2$  electrodes were recorded under UV-A illumination using several acetone concentrations (from 1 mM to 1 M) in the  $\text{N}_2$ -purged electrolyte solution.

## 2.5. Photocatalytic set-up

The photocatalytic degradation of acetone in air was conducted in a Pyrex glass cylindrical reactor with a diameter of 200 mm and an effective volume of 5 L. The amount of catalyst (in the form of powder deposited from a 2-propanol slurry on a flat glass disk) used in the tests was 0.05 g [34]. The gaseous mixture in the reactor was obtained by mixing hot chromatographic air, humidified at 40%, and a fixed amount of volatilized pollutant, in order to avoid condensation. The initial concentration of acetone in the reactor was 400 ppmv. The photon source was a 500 W iron halogenide lamp (Jelosil, model HG 500) emitting in the 315–400 nm wavelength range (UV-A) at  $30 \text{ W}\cdot\text{m}^{-2}$ . Acetone tests lasted for 2 h. The actual concentration of pollutant adsorbed on  $\text{TiO}_2$  in the reactor was determined directly by micro-GC sampling.

## 3. RESULTS AND DISCUSSION

### 3.1. Characterization of the Titania powders

The surface area of nano-sized powders, analyzed by means of the BET method, is higher than that of the micro-sized samples, as expected [14]. P25 and PC105 show a surface area of 50 and  $80 \text{ m}^2/\text{g}$ , respectively, while 1077 and AH-R show much lower values ( $\sim 12 \text{ m}^2/\text{g}$ ). The XRD spectra reveal the presence of the pure anatase phase for all the quoted samples, but P25, which contains a 75:25 ratio of anatase-to-rutile phase [35]. The morphological aspects of all samples were examined by HR-TEM (Fig. 1). Nanometric powders (P25 and PC105) exhibit the typical average particle size

of 20-30 nm. Furthermore, the nano-sized materials are homogeneous with well-packed crystalline particles. In parallel with this, a distinctive morphology could be noticed in the micrometric samples (1077 and AH-R). The average size falls into the 100-130 nm range, as confirmed by XRD. In all cases, the analyses of the fringe patterns (either as such or by means of the FFT elaboration) reveal the presence of the (101) family of planes ascribable to the anatase phase (ICDD card n. 21-1272). Finally, the average thickness of the respective films (as measured by profilometry in two different sections of the TiO<sub>2</sub> annealed film), was about 3 μm for both nanometric and micrometric samples.

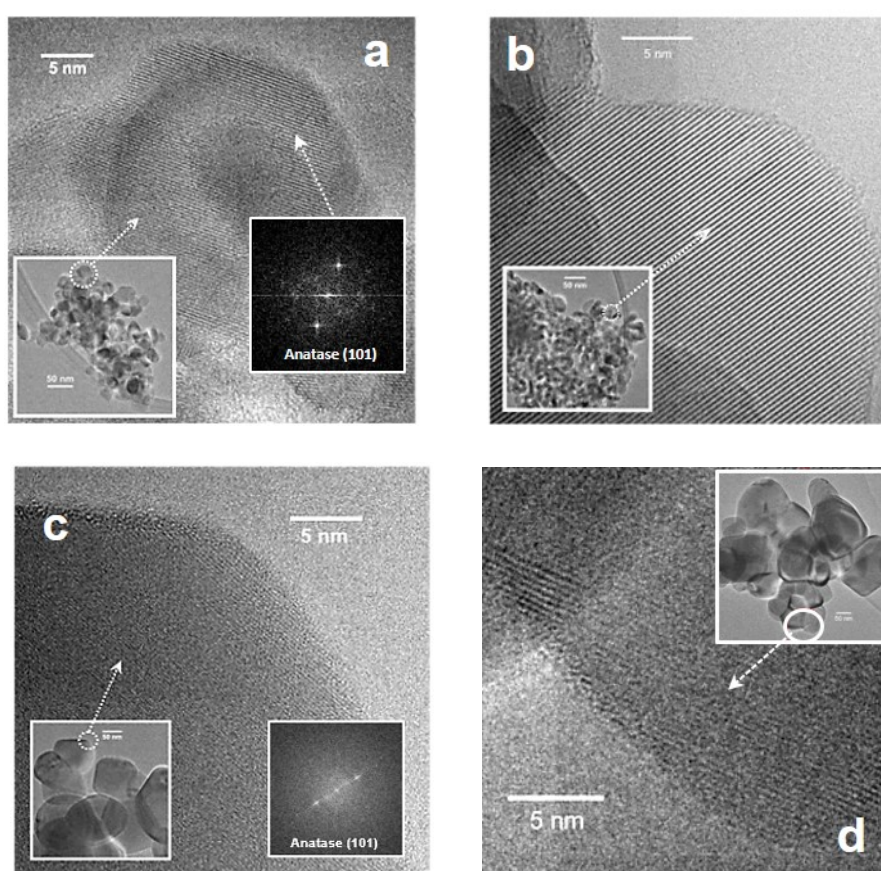


**FIGURE 1.** HR-TEM images of P25 (a) and PC105 (b) nano-sized samples; 1077 (c) and AH-R (d) micro-sized samples. Insets show: (i) a 50 nm scale image of the samples and (ii) fringe patterns FFT elaboration in the cases of (a) and (c) samples.

It is well known that surface hydroxyls are crucial species for the photocatalytic process. In particular, photo-generated holes may react with water molecules adsorbed on semiconductor surfaces, resulting in the formation of trapped holes as OH radicals [14]. To evince the prospective formation these radicals, FTIR spectra of the samples in the  $\nu(\text{OH})$  spectral range in air (black lines) and after outgassing at RT (red lines) are reported in Fig. 2. All the materials in air exhibit two complex absorption bands, respectively located in the  $3000\text{-}3450\text{ cm}^{-1}$  range and at  $\nu \geq 3600\text{ cm}^{-1}$ . On the basis of the spectral behavior and of the literature data [36, 37], the former broad peak can be ascribed to the stretching mode of all H-bonded OH groups present at the surface of the various solids, whereas the latter corresponds to the stretching mode of all Ti-OH species free from hydrogen bonding interactions. Comparing the spectra of nano-sized samples with that of micro-sized  $\text{TiO}_2$ , it is evident that nano-sized samples are characterized by a significantly higher amount of hydroxyl species. In particular, PC105 shows the highest amount of OH groups among the samples studied, where the absorbance of PC105 has been divided by 2. Moreover, nano-sized surface samples are characterized by an uneven distribution of terminal Ti-OH species in comparison with their micro-sized counterparts (1077 and AH-R).

After outgassing at RT (Fig. 2, red lines) physisorbed water molecules are removed and, as a consequence, the absorbance of the envelope related to H-bonded OH groups decreases significantly. For the micro-sized  $\text{TiO}_2$ , the band related to Ti-OH shifts toward lower frequency upon outgassing, indicating that physisorbed water alters the reactivity of Ti-OH groups. In particular, a band at lower frequency points to the presence of hydroxyl groups with a more acidic character.

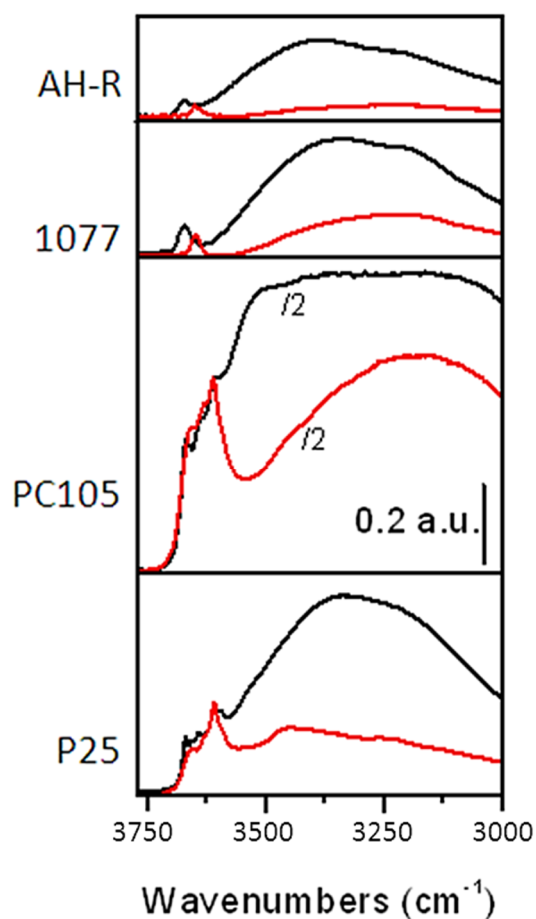
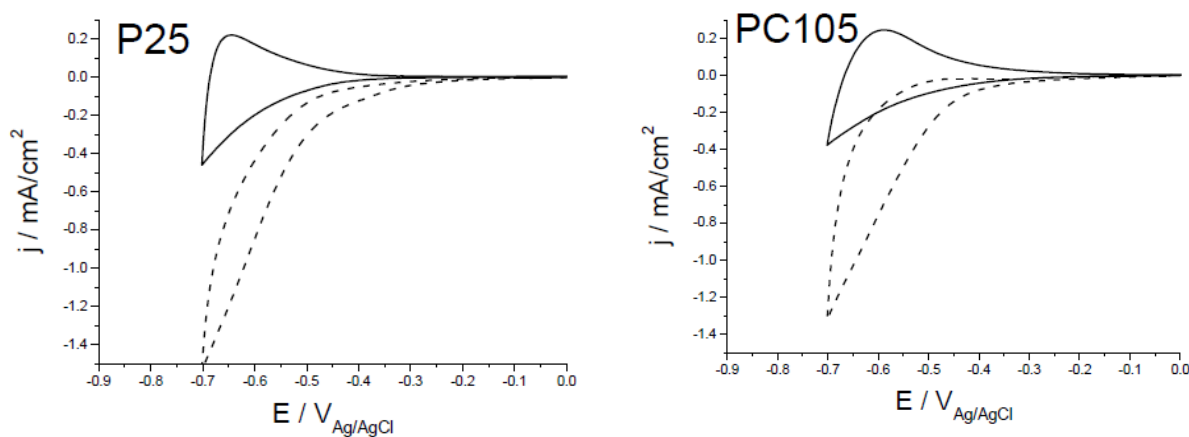


**FIGURE 2.** Absorbance IR spectra in the OH stretching region for the different samples (P25, PC105, 1077, AH-R) in air (black lines) and after outgassing at RT for 60 min (red lines). The absorbance depicted for PC105 sample has been divided by 2.

### 3.2. Photoelectrochemical analysis

In photo(electro)catalysis, two separate processes take place simultaneously: the oxidation process based on photogenerated hole transfer and the reduction process with photogenerated electrons, which can be separately studied, including their kinetics, by electrochemical methods. Moreover, it is of great interest to correlate the photoelectrochemical and photocatalytic behavior of the nanosized TiO<sub>2</sub> samples (P25 and PC105), in comparison with that of a microsized ones (AH-R and 1077).

Let us start with the oxygen reduction process. Recently, Berger et al. experimentally established that the accumulation region onset reflects the conduction band and surface state properties and that the associated current is correlated to the active surface area [38, 39]. Fig. 3 shows the voltammograms in the dark for nano- and micro-sized  $\text{TiO}_2$  samples in a 0.1 M  $\text{HClO}_4$  aqueous solution in the presence and the absence of oxygen. In the absence of oxygen, the voltammetric response is dominated by the accumulation region appearing at potentials below -0.2 V vs. Ag/AgCl. As expected, the capacitance of the nanocrystalline electrodes is much larger than that of the microcrystalline ones, as the interfacial area of the nanocrystalline electrodes is expected to be much larger for the same electrode thickness. The shown reductive currents are directly associated to the accumulation of electrons in the  $\text{TiO}_2$  film. Nanometric samples (P25 and PC105) show higher reductive currents in agreement with the literature, [40] which is likely related to the higher internal surface area of these samples with respect to microsized ones. In any case, the onset of the oxygen reduction current is similar in all cases and coincides with the onset of the accumulation region.



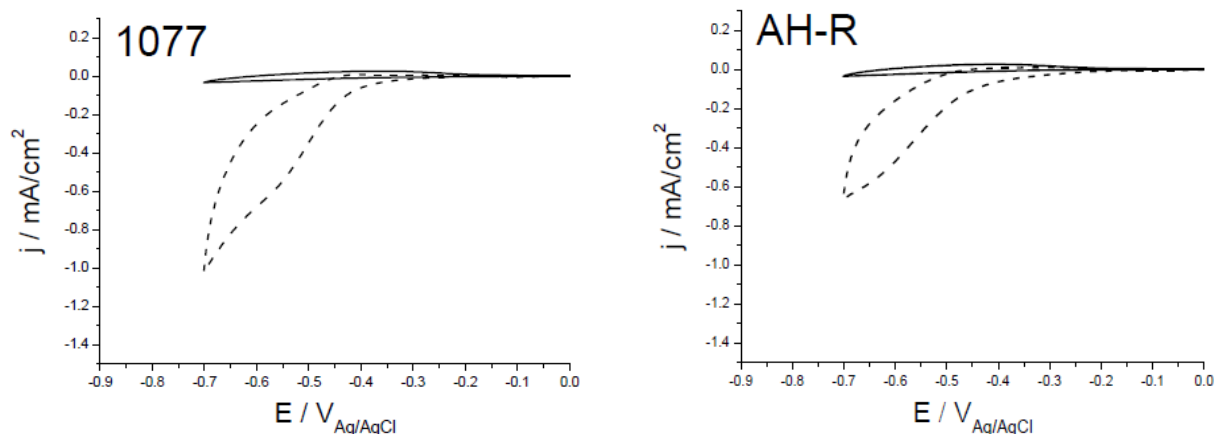


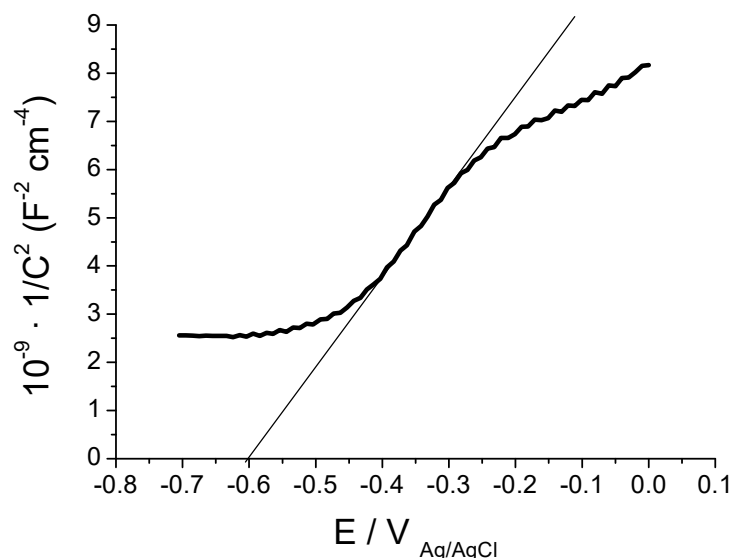
**FIGURE 3.** Voltammograms in the dark for nano-sized (P25 and PC105) and micro-sized (1077 and AH-R) electrodes in 0.1 M HClO<sub>4</sub> solution in the presence (---) and in the absence (—) of oxygen.

Prior to presenting and discussing the photoelectrochemical results, it is interesting to obtain information on the double layer structure in each of these types of electrodes. In the case of nanocrystalline electrodes, the existence of significant band bending within the particles is discarded, as their mesoporous nature and small particle diameter precludes the formation of a sizable in-built electric potential gradient. However, this is not necessary the case of microcrystalline electrodes.

For a deeper understand of the TiO<sub>2</sub> microcrystalline electrodes, the potential dependence of capacitance was analyzed using the Mott-Schottky (M-S) theory. A linear behavior in the  $C_{sc}^{-2}$  vs. E plot would point to the existence of a space charge layer within each particle. In addition, it would allow one to determine both the donor concentration,  $N_D$ , and the flatband potential,  $E_{fb}$ , of the semiconductor electrode. The relative equation is:

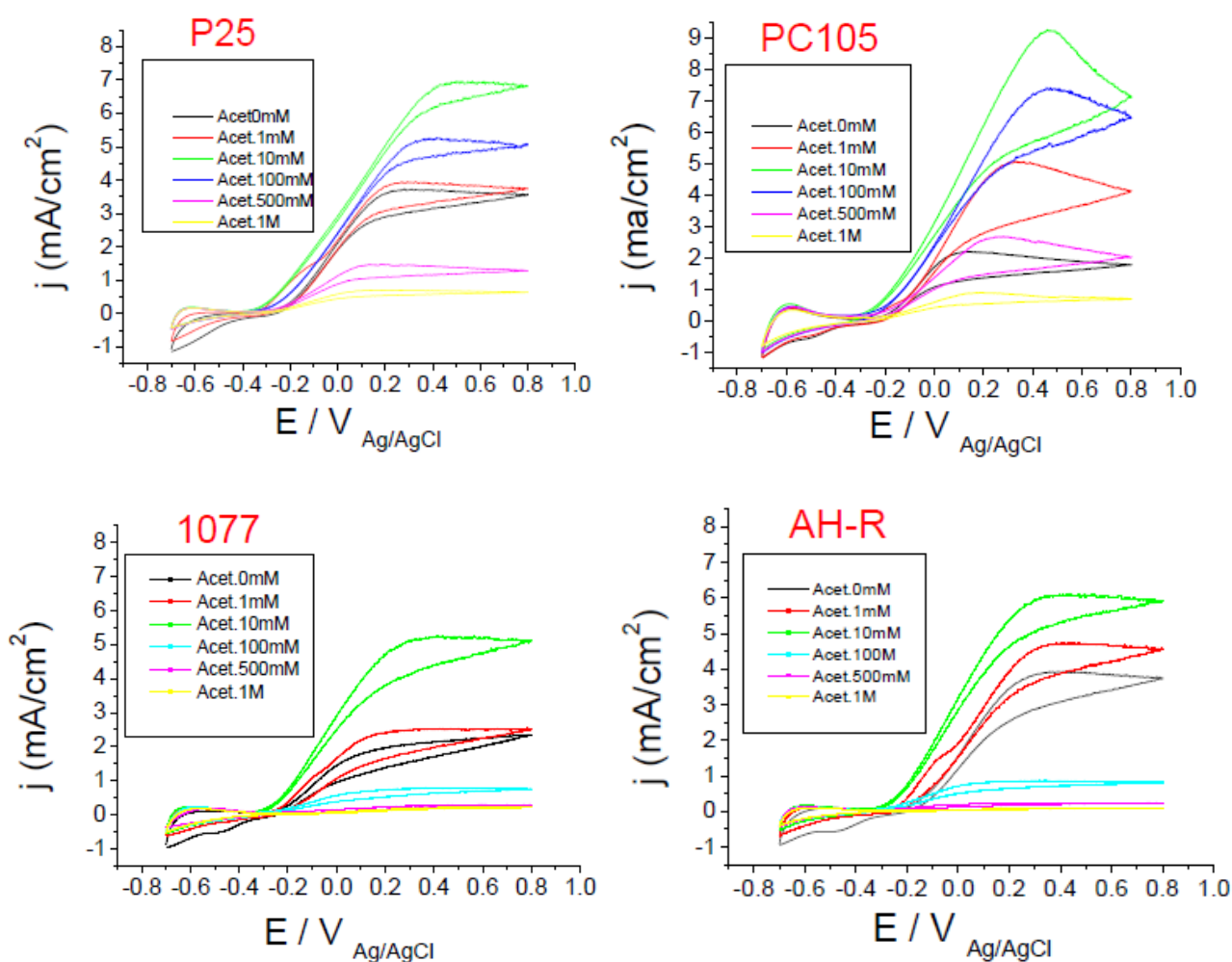
$$C_{sc}^{-2} = \left( \frac{2}{\epsilon \epsilon_0 e N_D} \right) (E - E_{fb} - kT/e)$$

where  $C_{sc}$  represents the differential capacitance of the space charge layer. The flat band potential is given by extrapolation to  $C^{-2} = 0$ . Fig. 4 shows the M-S plot for the micro-sized  $\text{TiO}_2$  electrode AH-R. A good linear correlation is found in a relatively wide potential range. This is interesting as it is compatible with the large particle size of AH-R sample sustaining a space charge layer. The value of  $E_{fb}$  results to be around -0.6 V.



**FIGURE 4.** Mott-Schottky plot for the micro-size electrode AH-R.

We shall focus now on the behavior of the different electrodes toward photooxidation processes. Fig. 5 shows voltammograms under UV illumination as a function of acetone concentration for all the samples under scope. The response in the absence of acetone is attributed to the photooxidation of water, while in its presence, the photooxidation of the organic compound should prevail. The latter can be deduced from the negative shift of the photocurrent onset observed upon the addition of acetone, which indicates that acetone photooxidation is easier than that of water, as the holes scavenging ability of acetone is much better than that of water, thus reducing the overpotential for its oxidation.

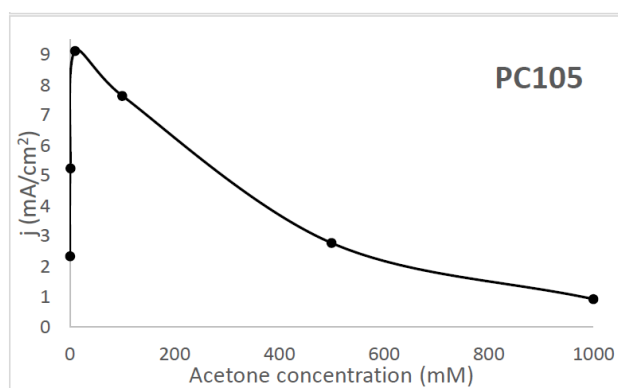
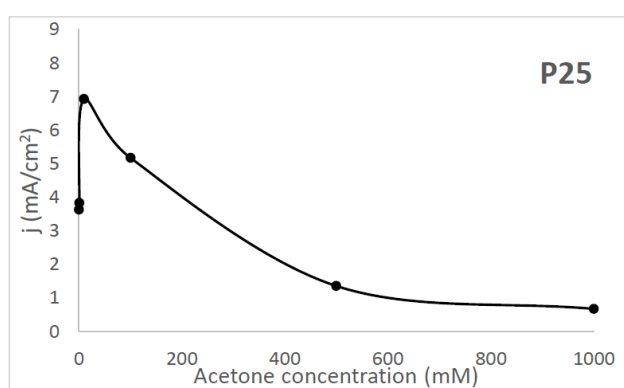


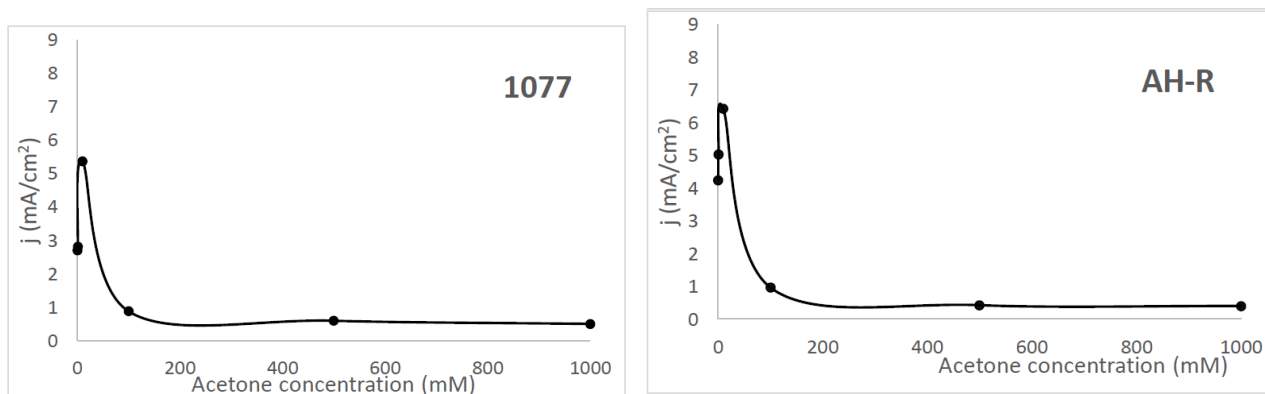
**FIGURE 5.** Voltammograms using UV light of nano-sized (P25 and PC105) and micro-sized samples (AH-Rand 1077) in 0.1 M HClO<sub>4</sub> and acetone at different concentrations.

Fig. 6 corresponds to the stationary photocurrent density (at 0.6 V) vs. acetone concentration plots for the same electrodes. The oxidation photocurrent increases with the concentration of acetone up to 10 mM and then decreases until a near-negligible photocurrent at 1 M of acetone. The values of the photocurrent under otherwise the same conditions depend on the TiO<sub>2</sub> type, but the characteristic trend is similar for all samples. The maximum current registered using 10 mM acetone for the nano TiO<sub>2</sub> samples, P25 and PC105, is in the range of 7-9 mA/cm<sup>2</sup>, whereas for 1077 and AH-R electrodes the values are slightly lower (5.5-6 mA/cm<sup>2</sup>). The adsorption of acetone on the surface of the TiO<sub>2</sub> film might be a reasonable cause for the trend observed for the photocurrent as the acetone

concentration in the electrolyte is increased. The addition of acetone (<10 mM) increases the photocurrent because either free or trapped holes react easily with the acetone adsorbed on TiO<sub>2</sub> allowing for an enhancement of the oxidative process. However, a further increase of the concentration of acetone gradually decreases the observed photocurrent maybe according to a strong adsorption of the pollutant that diminishes the formation of OH<sup>·</sup>. For acetone concentrations higher than 1 M, very low photocurrents can be recorded probably due to a complete inhibition of the anodic process by blocking the TiO<sub>2</sub> electrode surface.

Therefore, the oxidative activity of the prepared TiO<sub>2</sub> electrodes reaches a maximum when the acetone concentration is around 10 mM. These observations are in agreement with the inhibition of the formic acid photooxidation on TiO<sub>2</sub> resulting from the addition of relatively small amounts of acetone [42]. It is remarkable that the photocurrent onset is located at slightly more negative potentials in the case of nanosized samples indicating a lower recombination rate. In the case of microcrystalline electrodes (AH-R), the flatband potential as determined from the Mott-Schottky plot is located at potentials more negative (by more than 0.2 V) than the onset potential, which unveils that substantial recombination occurs even in the presence of the organics.





**FIGURE 6.** Photocurrent density plots vs. acetone concentration recorded at +0.6 V in 0.1M HClO<sub>4</sub> for nano-sized (P25 and PC105) and micro-sized electrodes (AH-R and 1077).

To gain more information about the potential activity of these powders as photocatalysts, in Fig. 7 the current density under illumination for the different TiO<sub>2</sub> electrodes corresponding to the photooxidation of acetone (dashed line) together with the current density in the dark corresponding to the reduction of oxygen (solid line) are plotted together. According to the Wagner-Traud principle, the intersection point gives the value of photocurrent (acetone oxidation) and dark current (oxygen reduction) under open circuit conditions (i.e., under the typical conditions of suspended photocatalysts). Fig. 7 shows that the P25 powder gives the fastest acetone oxidation of all the samples checked. PC105 and AH-R would have very similar photoactivities, while 1077, would show the lowest photoefficiency. The significant differences found among the different TiO<sub>2</sub> powders highlight that P25, thanks to its peculiar properties, like high surface area, the presence of rutile and the particle morphology, happens to show the best photoefficiency. In particular, we believe that P25 efficiency is highly enhanced by the presence of both phases. The offset between the energetic locations of the conduction band and valence band edges for rutile and anatase should favor charge separation and diminish recombination. In general, there are two opposite factors that should play a key role in determining the photoactivity of powdered TiO<sub>2</sub> samples and electrodes: (i) a high

interfacial area in nanocrystalline samples, which is particularly desirable in the case of substances present at low concentrations; and (ii) the existence of a space charge in microcrystalline samples, diminishing recombination and enhancing photoactivity. Because of the existence of these opposing factors, it is understandable that particular nanocrystalline and microcrystalline samples could exhibit similar photoactivities. Thus, according to our electrochemical measurements, the photoefficiency of the studied TiO<sub>2</sub> samples follows the trend: P25>PC105≈AHR>1077.

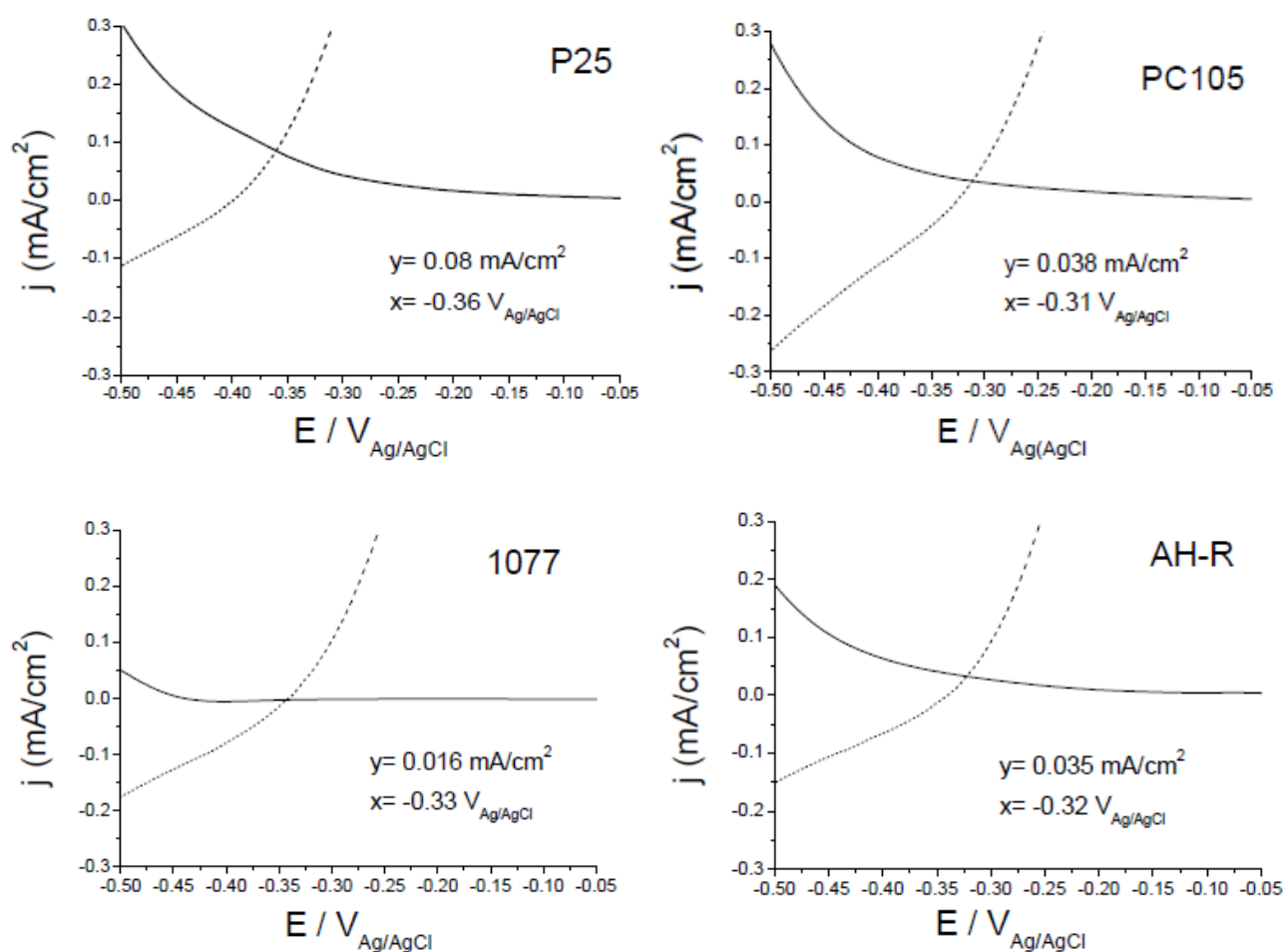


**FIGURE 7.** Current density plots for the TiO<sub>2</sub> electrodes on 0.1M HClO<sub>4</sub> + 10mM acetone solution corresponding to the photooxidation of acetone (-----) and the reduction of oxygen (—) in the dark (the latter, as its absolute value).

### 3.3. Photodegradation results

Photocatalytic processes are based on the high oxidative potential of photogenerated holes either free or at the catalyst surface. When the  $\text{TiO}_2$  is irradiated with UV light, electrons are promoted to the conduction band with the formation of holes on the valence band, leading to charge separation. These highly reactive species can promote oxidation and reduction reactions. The reaction of radical species generated through the capture of holes together with the direct transfer of holes, are the main steps in the photodegradation of many organic compounds, like acetone, adsorbed on the surface of  $\text{TiO}_2$ .

In Fig. 8, the degradation of acetone on the four studied  $\text{TiO}_2$  samples is reported. The photoefficiency of AHR is lower than the activity obtained to P25 and PC105 (nano-sized), that is in the sequence  $\text{P25} \approx \text{PC105} > 1077 > \text{AHR}$  with an inversion of the two micro-sized samples behavior as previously observed in the photoelectrochemical measures. Nano-sized samples show the best photocatalytic performance, leading to a complete degradation of acetone within 1 hour. A reason for the different photoactivity of AH-R, together to 1077, could be due to morphological differences, which reflect into a distribution of free ROSs including hydroxyl radicals, involved in the photooxidation as confirmed by FTIR characterization.

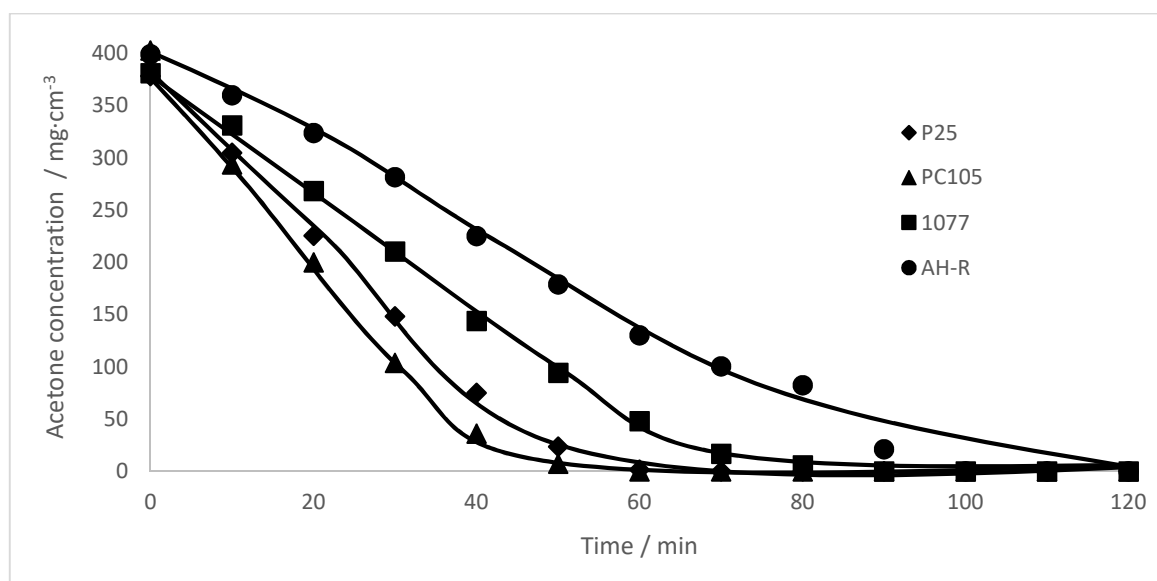


**FIGURE 8.** Photocatalytic acetone degradation with nano-sized (P25 and PC105) and micro-sized (1077 and AH-R) TiO<sub>2</sub> samples.

As previously reported by Bianchi et al. [14], the photodegradation of acetone in gas phase is highly influenced by the amount of OH available on the catalytic surface. In particular, Ti-OH-Ti bridged species play a crucial role for the photooxidation of chemical pollutants, such as acetone. In fact, a high amount of Ti-OH-Ti bridged moieties, located in the 3000-3450 cm<sup>-1</sup> range in the IR spectrum (see the spectra reported in Figure 2), leads to the best photodegradation result. Thus, nano-sized samples have the highest photocatalytic activity, because of the high degree of hydroxylation of their surfaces, as evidenced by the IR spectra. However, micro-sized TiO<sub>2</sub> still exhibits a photodegradation comparable to nanometric samples. To shed light on this issue, Fig. 9 reports the XPS spectra for both microcrystalline samples. Peak I is O1s attributed to bulk O while peaks II and III would correspond to bridging and terminal OH groups [43]. The ratio OH/O<sup>2-</sup> is 0.32 and 0.12, respectively for 1077 and AH-R. This dissimilarity between the two micro-sized powders confirms the fundamental role of ·OH radicals in the photocatalytic process, and explains the faster photooxidation with 1077 (see Fig. 8).

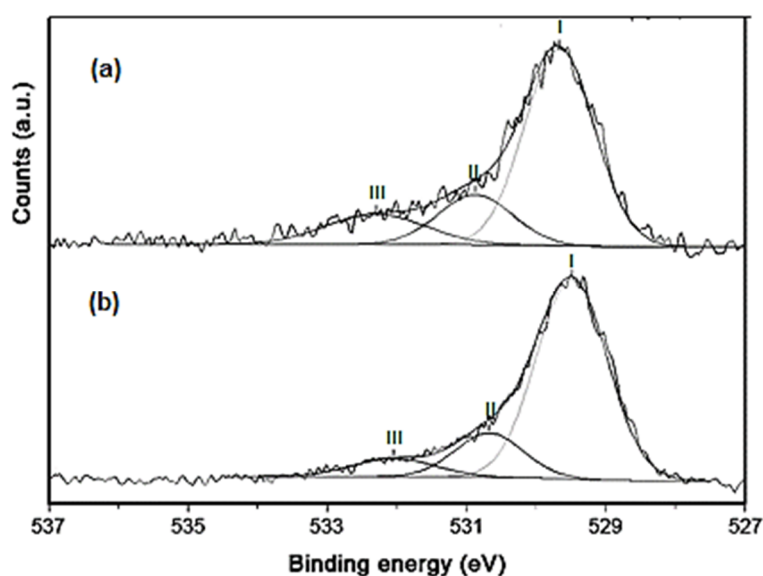


**FIGURE 9.** XPS spectra in the O1s region for (a) 1077 and (b) AH-R.

#### 4. CONCLUSIONS

Photoelectrochemical and photocatalytic studies were conducted on nano- and micro-sized TiO<sub>2</sub> commercial samples. The comparison was conducted for the photodegradation of acetone, a typical indoor pollutant. It was found that a high concentration of pollutant inhibits the photoelectrodegradation measure. Importantly, both nano- and micro-sized TiO<sub>2</sub> samples revealed that the optimal concentration for the oxidation of acetone was close to 10 mM. By comparing both kinds of samples, nanometric samples were found to exhibit higher photocurrents than micro-sized ones. The photoelectrocatalytic activity of the samples was evaluated by comparing the j-E curves obtained in the presence of oxygen in the dark and in the presence of acetone (10 mM) under UV illumination. The best efficiency was obtained for nanometric P25, which generates an equivalent photocurrent under open circuit conditions higher (0.08 mA/cm<sup>2</sup>) than the other ones. Otherwise, both nano-sized PC105 and micro-sized AH-R have the similar values of photocurrent (0.03 mA/cm<sup>2</sup>), resulting more active than the other micrometric sample (1077). It is remarkable that a nanocrystalline and a microcrystalline sample display similar efficiency. This is a result of the existence of two separate factors: increased surface area (in nanosized samples) and the existence of an operating space charge layer (in micro-sized samples). Among the different TiO<sub>2</sub> samples, PC105 and P25 exhibit the best results in photocatalytic gaseous oxidation. On the contrary, 1077 has better photoefficiency than AH-R, evidenced by the faster oxidation rate. This feature could be explained by the amount of photoactive “free” Ti-OH sites, which are probably responsible of photooxidation. In summary, it is important to highlight that micro-sized samples have different behaviors depending on the catalytic processes. In photoelectrochemical analysis, not only the degree of hydroxylation but also the morphology and the particle size play an important role while for the photocatalysis in gas phase, OH

radicals have a fundamental role. In this sense, micro-sized TiO<sub>2</sub> samples could be valuable candidates for the photooxidation of VOC in gas phase.

## ACKNOWLEDGEMENTS

R.G. and P.B. are grateful to the Spanish Ministry of Economy and Competitiveness for financial support through project MAT2012-37676 (Fondos FEDER).

## REFERENCES

- [1] J. Schneider, M. Matsuoka, M. Takeuchi, J. Zhang, Y. Horiuchi, M. Anpo, D.W. Bahnemann, Understanding TiO<sub>2</sub> photocatalysis: mechanisms and materials, *Chemical reviews*, 114 (2014) 9919-9986.
- [2] R. Djellabi, M.F. Ghorab, A. Smara, C.L. Bianchi, G. Cerrato, X. Zhao, B. Yang, Titania–Montmorillonite for the Photocatalytic Removal of Contaminants from Water: Adsorb & Shuttle Process, *Green Materials for Wastewater Treatment*, Springer 2020, pp. 291-319.
- [3] R. Fagan, D.E. McCormack, D.D. Dionysiou, S.C. Pillai, A review of solar and visible light active TiO<sub>2</sub> photocatalysis for treating bacteria, cyanotoxins and contaminants of emerging concern, *Materials Science in Semiconductor Processing*, 42 (2016) 2-14.
- [4] X. Kang, S. Liu, Z. Dai, Y. He, X. Song, Z. Tan, Titanium dioxide: from engineering to applications, *Catalysts*, 9 (2019) 191.
- [5] G.V. Lowry, K.B. Gregory, S.C. Apte, J.R. Lead, *Transformations of nanomaterials in the environment*, ACS Publications, 2012.
- [6] Y. Nam, J.H. Lim, K.C. Ko, J.Y. Lee, Photocatalytic activity of TiO<sub>2</sub> nanoparticles: a theoretical aspect, *Journal of Materials Chemistry A*, 7 (2019) 13833-13859.
- [7] J. Hou, L. Wang, C. Wang, S. Zhang, H. Liu, S. Li, X. Wang, Toxicity and mechanisms of action of titanium dioxide nanoparticles in living organisms, *Journal of environmental sciences*, 75 (2019) 40-53.
- [8] S. Park, S. Lee, B. Kim, S. Lee, J. Lee, S. Sim, M. Gu, J. Yi, J. Lee, Toxic effects of titanium dioxide nanoparticles on microbial activity and metabolic flux, *Biotechnology and bioprocess engineering*, 17 (2012) 276-282.
- [9] E. Baranowska-Wójcik, D. Sz wajgier, P. Oleszczuk, A. Winiarska-Mieczan, Effects of titanium dioxide nanoparticles exposure on human health—A review, *Biological trace element research*, 193 (2020) 118-129.
- [10] K. Oravisjärvi, M. Pietikäinen, J. Ruuskanen, A. Rautio, A. Voutilainen, R.L. Keiski, Effects of physical activity on the deposition of traffic-related particles into the human lungs in silico, *Science of the total environment*, 409 (2011) 4511-4518.
- [11] J. Ai, E. Biazar, M. Jafarpour, M. Montazeri, A. Majdi, S. Aminifard, M. Zafari, H.R. Akbari, H.G. Rad, Nanotoxicology and nanoparticle safety in biomedical designs, *International journal of nanomedicine*, 6 (2011) 1117.
- [12] S. Xiong, S. George, Z. Ji, S. Lin, H. Yu, R. Damoiseaux, B. France, K.W. Ng, S.C.J. Loo, Size of TiO<sub>2</sub> nanoparticles influences their phototoxicity: an in vitro investigation, *Archives of toxicology*, 87 (2013) 99-109.

- [13] K. Cai, Y. Hou, Y. Hu, L. Zhao, Z. Luo, Y. Shi, M. Lai, W. Yang, P. Liu, Correlation of the cytotoxicity of TiO<sub>2</sub> nanoparticles with different particle sizes on a sub - 200 - nm scale, *Small*, 7 (2011) 3026-3031.
- [14] C. Bianchi, S. Gatto, C. Pirola, A. Naldoni, A. Di Michele, G. Cerrato, V. Crocellà, V. Capucci, Photocatalytic degradation of acetone, acetaldehyde and toluene in gas-phase: comparison between nano and micro-sized TiO<sub>2</sub>, *Applied Catalysis B: Environmental*, 146 (2014) 123-130.
- [15] C.L. Bianchi, B. Sacchi, C. Pirola, F. Demartin, G. Cerrato, S. Morandi, V. Capucci, Aspirin and paracetamol removal using a commercial micro-sized TiO<sub>2</sub> catalyst in deionized and tap water, *Environmental Science and Pollution Research*, 24 (2017) 12646-12654.
- [16] C.L. Bianchi, E. Colombo, S. Gatto, M. Stucchi, G. Cerrato, S. Morandi, V. Capucci, Photocatalytic degradation of dyes in water with micro-sized TiO<sub>2</sub> as powder or coated on porcelain-grès tiles, *Journal of Photochemistry and Photobiology A: Chemistry*, 280 (2014) 27-31.
- [17] R. Djellabi, M.F. Ghorab, T. Sehili, Simultaneous removal of methylene blue and hexavalent chromium from water using TiO<sub>2</sub>/Fe(III)/H<sub>2</sub>O<sub>2</sub>/sunlight, *CLEAN–Soil, Air, Water*, 45 (2017) 1500379.
- [18] S. Chen, S.S. Thind, A. Chen, Nanostructured materials for water splitting-state of the art and future needs: A mini-review, *Electrochemistry Communications*, 63 (2016) 10-17.
- [19] S. Ho-Kimura, S.J. Moniz, A.D. Handoko, J. Tang, Enhanced photoelectrochemical water splitting by nanostructured BiVO<sub>4</sub>-TiO<sub>2</sub> composite electrodes, *Journal of Materials Chemistry A*, 2 (2014) 3948-3953.
- [20] T. Jafari, E. Moharrerri, A.S. Amin, R. Miao, W. Song, S.L. Suib, Photocatalytic water splitting—the untamed dream: a review of recent advances, *Molecules*, 21 (2016) 900.
- [21] P. Szymanski, M.A. El-Sayed, Some recent developments in photoelectrochemical water splitting using nanostructured TiO<sub>2</sub>: a short review, *Marco Antonio Chaer Nascimento, Springer*2014, pp. 7-18.
- [22] L. Mais, M. Mascia, S. Palmas, A. Vacca, Photoelectrochemical oxidation of phenol with nanostructured TiO<sub>2</sub>-PANI electrodes under solar light irradiation, *Separation and Purification Technology*, 208 (2019) 153-159.
- [23] V.V. Kondalkar, S.S. Mali, R.M. Mane, P. Dandge, S. Choudhury, C.K. Hong, P.S. Patil, S.R. Patil, J.H. Kim, P.N. Bhosale, Photoelectrocatalysis of cefotaxime using nanostructured TiO<sub>2</sub> photoanode: identification of the degradation products and determination of the toxicity level, *Industrial & Engineering Chemistry Research*, 53 (2014) 18152-18162.
- [24] Y. Tang, H. Ren, J. Huang, Synthesis of porous TiO<sub>2</sub> nanowires and their photocatalytic properties, *Frontiers of Optoelectronics*, 10 (2017) 395-401.
- [25] J. Zhang, R. Djellabi, S. Zhao, M. Qiao, F. Jiang, M. Yan, X. Zhao, Recovery of phosphorus and metallic nickel along with HCl production from electroless nickel plating effluents: the key role of three-compartment photoelectrocatalytic cell system, *Journal of Hazardous Materials*, (2020) 122559.
- [26] J. Zhang, X. Zhao, Y. Wang, R. Djellabi, Recovery of Phosphorus from Hypophosphite-Laden Wastewater: A Single-Compartment Photoelectrocatalytic Cell System Integrating Oxidation and Precipitation, *Environmental Science & Technology*, (2019).
- [27] D. Monllor-Satoca, T. Lana-Villarreal, R. Gómez, Effect of surface fluorination on the electrochemical and photoelectrocatalytic properties of nanoporous titanium dioxide electrodes, *Langmuir*, 27 (2011) 15312-15321.
- [28] Y.J. Hwang, C. Hahn, B. Liu, P. Yang, Photoelectrochemical properties of TiO<sub>2</sub> nanowire arrays: a study of the dependence on length and atomic layer deposition coating, *ACS nano*, 6 (2012) 5060-5069.
- [29] T. Ochiai, A. Fujishima, Photoelectrochemical properties of TiO<sub>2</sub> photocatalyst and its applications for environmental purification, *Journal of Photochemistry and photobiology C: Photochemistry reviews*, 13 (2012) 247-262.

- [30] P. Acevedo-Peña, I. González, Relation between morphology and photoelectrochemical performance of TiO<sub>2</sub> nanotubes arrays grown in ethylene glycol/water, *Procedia Chem*, 12 (2014) 34-40.
- [31] H. Ennaceri, K. Fischer, K. Hanus, A. Chemseddine, A. Prager, J. Griebel, M. Kühnert, A. Schulze, B. Abel, Effect of Morphology on the Photoelectrochemical Activity of TiO<sub>2</sub> Self-Organized Nanotube Arrays, *Catalysts*, 10 (2020) 279.
- [32] M. Ibadurrohman, K. Hellgardt, Morphological modification of TiO<sub>2</sub> thin films as highly efficient photoanodes for photoelectrochemical water splitting, *ACS applied materials & interfaces*, 7 (2015) 9088-9097.
- [33] T. Lana-Villarreal, Y. Mao, S.S. Wong, R. Gómez, Photoelectrochemical behaviour of anatase nanoporous films: effect of the nanoparticle organization, *Nanoscale*, 2 (2010) 1690-1698.
- [34] C.L. Bianchi, C. Pirola, E. Selli, S. Biella, Photocatalytic NO<sub>x</sub> abatement: the role of the material supporting the TiO<sub>2</sub> active layer, *Journal of hazardous materials*, 211 (2012) 203-207.
- [35] R.I. Bickley, T. Gonzalez-Carreno, J.S. Lees, L. Palmisano, R.J. Tilley, A structural investigation of titanium dioxide photocatalysts, *Journal of Solid State Chemistry*, 92 (1991) 178-190.
- [36] R. Djellabi, B. Yang, Y. Wang, X. Cui, X. Zhao, Carbonaceous biomass-titania composites with TiOC bonding bridge for efficient photocatalytic reduction of Cr(VI) under narrow visible light, *Chemical Engineering Journal*, 366 (2019) 172-180.
- [37] R. Djellabi, B. Yang, K. Xiao, Y. Gong, D. Cao, H.M.A. Sharif, X. Zhao, C. Zhu, J. Zhang, Unravelling the mechanistic role of TiOC bonding bridge at titania/lignocellulosic biomass interface for Cr(VI) photoreduction under visible light, *Journal of colloid and interface science*, 553 (2019) 409-417.
- [38] T. Berger, T. Lana-Villarreal, D. Monllor-Satoca, R. Gómez, Thin films of rutile quantum-size nanowires as electrodes: Photoelectrochemical studies, *The Journal of Physical Chemistry C*, 112 (2008) 15920-15928.
- [39] M. Jankulovska, I. Barceló, T. Lana-Villarreal, R. Gómez, Improving the photoelectrochemical response of TiO<sub>2</sub> nanotubes upon decoration with quantum-sized anatase nanowires, *The Journal of Physical Chemistry C*, 117 (2013) 4024-4031.
- [40] L.A. Lyon, J.T. Hupp, Energetics of semiconductor electrode/solution interfaces: EQCM evidence for charge-compensating cation adsorption and intercalation during accumulation layer formation in the titanium dioxide/acetonitrile system, *The Journal of Physical Chemistry*, 99 (1995) 15718-15720.
- [41] T. Berger, D. Monllor - Satoca, M. Jankulovska, T. Lana - Villarreal, R. Gómez, The electrochemistry of nanostructured titanium dioxide electrodes, *ChemPhysChem*, 13 (2012) 2824-2875.
- [42] R. Morand, C. Lopez, M. Koudelka-Hep, P. Kedzierzawski, J. Augustynski, Photoelectrochemical behavior in low-conductivity media of nanostructured TiO<sub>2</sub> films deposited on interdigitated microelectrode arrays, *The Journal of Physical Chemistry B*, 106 (2002) 7218-7224.
- [43] E. Bullock, L. Patthey, S. Steinemann, Clean and hydroxylated rutile TiO<sub>2</sub> (110) surfaces studied by X-ray photoelectron spectroscopy, *Surface science*, 352 (1996) 504-510.